ASTRONOMY
AND
ASTROPHYSICS

A stellar coronograph
for the COME-ON-PLUS adaptive optics system[*]

II. First astronomical results

D. Mouillet[1], A.-M. Lagrange[1], J.-L. Beuzit[1,2], and N. Renaud[1]

[1] Laboratoire d'Astrophysique de l'Observatoire de Grenoble, UMR 5571, Université J. Fourier, BP 53, F-38041 Grenoble Cedex 9, France
[2] DESPA, Observatoire de Paris, URA 264, Place J. Janssen, F-92195 Meudon Cedex, France

Abstract. We present here the first scientific results obtained with the coronograph described by Beuzit et al. (1996, hereafter paper I), developed to be used together with the COME-ON-PLUS/ADONIS adaptive optics (AO) system. Two IRAS excess Main Sequence (MS) stars, namely HR 4796 and HR 2020 (β Pictoris), have been observed.

No circumstellar disk is detected around HR 4796, down to $2''$ from the star. This new constraint on its circumstellar environment is discussed. The photometry in the J, H, and K bands allows us to derive a G0 to G2 spectral type for a faint companion located at $4.7''$.

The βPictoris disk is detected through scattered light as close as $1.5''$ from the star. We derive the radial mid-plane brightness from $1.5''$ to $6''$, and the FWHM from $2''$ to $6''$. We compare our results with other observations: here, the disk appears thinner than previously, and its surface brightness radial distribution gets flatter in the inner part. These results are then discussed in terms of density of the circumstellar matter.

Key words: stars: circumstellar matter – stars: imaging – stars: individual: β Pictoris

1. The circumstellar environment of HR 4796

1.1. Scientific context

HR 4796A (V = 6) is an IRAS excess A0V star, located at 76 pc. Among the IRAS excess MS stars, it exhibits a very strong disk luminosity ($L_{IR}/L_\odot = 5\,10^{-3}$), even higher than the β Pictoris one (Jura 1991). It is also probably a member of a multiple system (Jura et al. 1993): at $7.7''$ from HR 4796A, HR 4796B (M4) is likely to be a real physical companion, contrary to HR 4796C, at $40''$, which is a background star. The study of such multiple

systems might then yield important clues to the scenario of disk formation in binary or multiple systems (Clarke & Pringle 1991; Artymowicz et al. 1991). Various observations of HR 4796B indicate that this star is still above the Main Sequence and allow an estimate of $3.\,10^6$ years for the age of the binary system. The strong IR excess may be connected with the youth of the system, if the observed circumstellar dust is a remnant of the protostellar nebula. Assuming such an age, grain lifetime considerations seem to indicate that the grains are larger than $3 - 10\,\mu$m, consistently with their blackbody behaviour between the 20 and 60 μm emissions. This size is much larger than that of interstellar grains. Jura et al. (1995) proposed that the observed grains have significantly grown up via coalescence. Lifetime considerations, together with sub-millimeter (800 μm) and IRAS data lead to an estimation of about 10^{27}g for the mass of dust, which is similar to the β Pictoris case (Zuckerman and Becklin 1993). Such a mass is comparable to the Earth mass.

Moreover, Jura et al. (1995) put some constraints on the location of the far IR emission. On the one hand, the 20 μm emission appears point-like in a 5.4 $''$ beam. On the other hand, they suggested that the grains are orbiting HR 4796A at characteristic distances ≥ 40 AU ($0.5''$) at least, since an inner void of matter is required to satisfy the IRAS color indications of a 110 K blackbody emission, in the case of an optically thin disk. Therefore, the dust responsible for the large IR emission centered on HR 4796A should be located between 40 and 300 AU, but has still to be imaged. Jura et al. (1995) proposed that a companion could be responsible for the inner void of matter. Such an object is theoretically expected to be located between 20 and 100 AU, and it must be lighter than 0.125 $M_\odot$ since it was not detected by speckle 2 μm observations.

Meanwhile, recent coronographic observations revealed another possible companion at less than $5''$, that will be referred to as HR 4796D (Kalas and Jewitt, 1993). No color information was yet available.

Our coronographic system (described in paper I) allows us to investigate the close (2–6$''$) environment of HR 4796A, down

Fig. 1. Observation of the IR excess MS star HR4796 (V = 6) with a 0.8"
mask in the K' band, with a 10 minute exposure time. The field-of-view
is 13"× 13" with a sampling of 0.05" per pixel, smoothed to 0.15". In
addition to the bright (K = 8.4) companion HR 4796B located at 7.6",
a faint companion (K = 14.5) HR 4796D is clearly detected at about
4.7" from the central star. No disk is detected down to a level of K =
20 mag arcsec^{-2}, neither any point like companion brighter than K =
14.6 mag, further than 2".

Table 1. Photometric measurements of the faint companion (HR
4796D) in the J, H, K' bands. They are relative to the photometry
of HR 4796B given by Jura et al. (1993). Uncertainties are of 0.2 mag,
due to the whole reduction procedure.

Object	P.A.	Distance from HR 4796A	J	H	K'
HR4796B	224	7.6"	9.3	8.6	8.4
HR4796D	311	4.7"	15.3	14.7	14.5

to much fainter detection limits than previously achieved. The
observations are presented in Sect. 1.2. Results on HR 4796D
and new observational constraints on the origin of IR emissions
are derived in Sect. 1.3.

1.2. Observations

HR 4796A was observed twice with the
COME-ON-PLUS/ADONIS adaptive optics system equipped with
our coronograph, on the ESO 3.6-meter telescope (La Silla,
Chile). In March 94, we used a 2" diameter occulting mask to
obtain images in the K' band (2.2 μm). And, in March 95, a 0.8"
diameter mask allowed to improve the K' observations and to
extend them to the J (1.25 μm) and H (1.65 μm) bands. The total
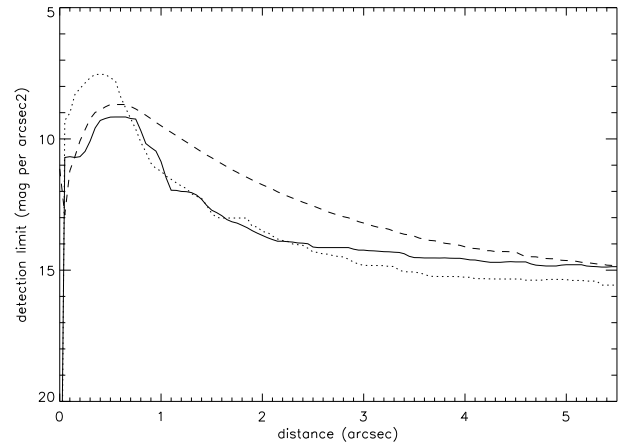exposure times were 10 minutes per filter. A comparison star,

Fig. 2. Detection limit as a function of the distance from HR 4796A,
in the J (dashed line), H (dotted line) and K' (full line) filters. The total
exposure time in each filter is 10 minutes. This limit corresponds to
the surface brightness limit per pixel. It is estimated as the rms residual
flux per pixel after the whole procedure on a emission free area, where
no signal should remain. It is expressed in terms of surface brightness
in mag arcsec^{-2}. The detection limit, estimated over a larger area, is
much better in terms of surface brightness.

HR 4879 (B8V, V = 6.0), was recorded in the same observing
conditions. Fig. 1 gives an example of our observations.

The reduction procedure is described in paper I; it allows in
particular to quantify the precision of the whole procedure and
derive a detection limit in terms of surface brightness (Fig. 2).

1.3. Results

1.3.1. HR 4796D

A faint companion is clearly detected at 4.7" from HR 4796A,
at the position angle P.A. = 311°, consistent with previous data
obtained in R band by Kalas and Jewitt (1993). The detection is
unambiguous and, noticeably, would have been possible down
to 2" from the star.

Table 1 gives the photometry of HR 4796D, in J, H and K'
bands, relative to that of HR 4796B given by Jura et al. (1993);
the uncertainty in this photometry comes from the residuals
after subtraction of the reference star (see paper I) and from the
determination of the scaling factor to be applied. Compared to
this uncertainty, the difference of the shape of the PSF between
HR 4796B and D, due to anisoplanatism, is negligible.

From these colors, we deduce a spectral type ranging be-
tween G0 and G2 (Koornneef 1983). Meanwhile, this star is 6
mag fainter than HR 4796B, whose spectral type is about M2.
This clearly indicates that HR 4796D is a background star and
then has no effect on the status and evolution of the HR 4796A
environment.

1.3.2. Close perturbing companion

A massive object located between 20 and 100 AU, suggested by
Jura et al. (1995) as a possible origin for an inner void close to

the star, was not detected via speckle observations down to K = 9.7, in this area (same reference).

Our observations of HR 4796A out of the occulting mask confirms this non detection with the 3σ limit of K = 8 at 20 AU, K = 10 at 40 AU and K = 12 at 80 AU respectively.

The use of the coronograph also allows us to constrain more precisely the region further than 115 AU. We believe that it is quite pertinent to explore this region, since the location of the possible massive object is not precisely known. We do not detect any perturbing companion of K $\leq$ 14.6 further than $2''$ (150 AU), or K $\leq$ 11 between $1.5''$ (115 AU) and $2''$.

If the inner void of dust close to the star suggested by the IRAS colors is generated by a massive object, upper masses are strongly constrained. Assuming the $3. \, 10^6$ age estimation (Jura et al., 1995), theoretical models (Burrows et al., 1993) enable us to give corresponding mass limits to former magnitude limits: $0.125 \, M_\odot$ closer than 80 AU (K $\leq$ 9.7) and a sub-stellar mass limit of $0.03 \, M_\odot$ further out (K $\leq$ 12).

However, one has to keep in mind that, first the inner void has not yet been directly detected, and secondly a close perturbing companion may not be the single explanation for the clearing process. Other clearing processes, such as radiation pressure and grain collisions, or different grain optical properties, could be involved to explain the IRAS fluxes. This assumption should remain under discussion, in comparison with other clearing processes or low grain emitting properties, because of the lack of direct detection.

1.3.3. Extended emission

Very interestingly, we do not detect either any signature of the presence of dust, down to a 3σ limit of 20.3 mag arcsec^{-2} for an emission extended over 1 arcsec^2 area (which means 400 pixels here), as close as 150 AU from the star. However, the IR excess is very large, even larger than that of β Pictoris. For instance, if the β Pictoris disk, already imaged up to 800 AU, was scaled to the distance and to the IR luminosity of HR 4796A, it would be 19.5 mag arcsec^{-2} at $2''$ from the star, and thus such a disk would be detected by the present observations. Then, we conclude that the dust environment responsible for the IR excess around HR 4796A significantly differs from that of β Pictoris.

There are several possible explanations:
(i) the dust cannot be detected with our observations and our reduction procedure if the distribution is spherical. However, a large amount of dust around the star is expected to shape a disk, especially if it is composed of large grains possibly in interaction in a coalescence growth mechanism.
(ii) the disk of dust is seen pole on: this would also be an unfavourable configuration for our techniques. Yet, the large v sini of HR 4796A (≥ 100 km s^{-1}) derived from our spectroscopic data, argues against such an orientation.
(iii) the grains are confined within our present $2''$ (150 AU) limit of confident investigation. This constraint together with the inner limit (40 to 200 AU) given by Jura et al. (1995) only leaves a narrow possible location for this dust. Such an a priori surprisingly narrow location is possibly related to the system binarity:
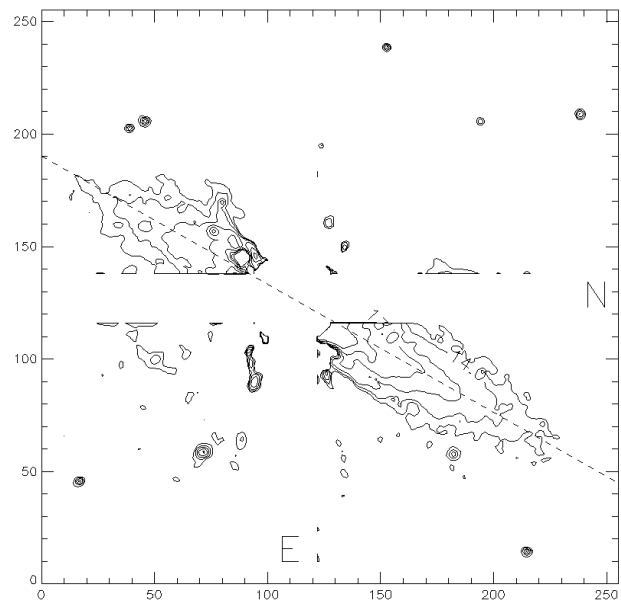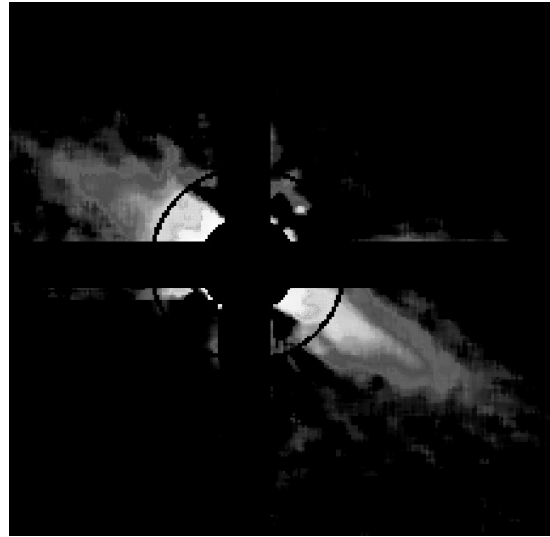

Fig. 3. Observation of the close environment of β Pictoris in December 1994. This image (top) corresponds to a total integration time of 6 minutes in the K' band. The field-of-view is $13'' \times 13''$ with a sampling of 0.05" per pixel, smoothed to 0.15". Quantitative measurements are possible down to 1.5" from the star, whereas uncorrected images provide information only down to 3" and tip–tilt correction or anti-blooming detectors provide quantitative information down to 2.4". Regularly spaced isophotes (bottom) are given from 12 to 14.5 mag arcsec^{-2}.

independent theoretical calculations of the gravitational stability in a binary system predict that the lifetime of a test particle further than one third of the distance between both stars is very short (Artymovicz & Lubow 1994). However, we have to note that precise constraints are uncertain here since we only know the projected distance of HR 4796B.
(iv) the grain properties can be very different from those around β Pictoris. Indeed, the scattering efficiency strongly depends on their size and nature.

One has to keep in mind that the indications on the location and shape of the dust proposed by Jura et al. (1995) are indirect and preliminary. They are derived from IR *unresolved* observations. Some of them are also based on lifetime considerations, which assume that the dust is as old as the stellar system and that the age of this system is precisely known. But, in the case of β Pictoris, for instance, similar lifetime considerations lead to the conclusion that no sub-μm particles should be present; however, near and far IR photometry and spectrophotometry actually indicate the presence of such grains (Harper et al. 1984, Backman et al. 1992, Knacke et al. 1993) and thus show that processing of dust is occurring there. Direct observational indications, such as thermal IR imaging, would be required to test those assumptions. New high angular resolution observations are needed to image with a better S/N the inner region down to 1.5″.

2. The β Pictoris disk

2.1. Scientific context

The β Pictoris disk was first detected through coronographic imaging of the scattered visible light (Smith & Terrile 1984). Since then, it has been studied in many different ways: imaging brought complementary information on the disk dust in scattered light as well as in thermal IR (Lagage & Pantin 1994); spectroscopic studies also enabled the investigation of the gaseous counterpart and very interestingly showed evidence of the presence of large solid bodies close to the star (Lagrange et al. 1995 and references therein). Each technique brings specific indications but has its own limitations. Up to now, optical imaging probed only the outer part of the disk; thermal IR photometry and spectroscopy probes the closest part but without imaging capabilities. In order to constrain both the density distribution and grain properties close to the star, one needs high angular resolution imaging, at various wavelengths.

We present and analyze here observations of the close environment of β Pictoris, obtained with our coronograph, coupled with the COME-ON-PLUS/ADONIS adaptive optics system.

2.2. Observations and reduction procedure

The observations of β Pictoris were performed on December 22, 1994 and March 23, 1995 using the K' filter. The occulting mask was 0.8″ in diameter. The atmospheric turbulence conditions were better and more stable on December 22, 1994. Two calibration reference stars were used: HR 2435 (A0II, V = 4.39) and HR 2550 (A7IV, V = 3.3). The individual exposures were 2s long, and the total integration time on β Pictoris was 6 minutes (Fig. 3).

Paper I describes the instrumental configuration and the general reduction procedure applied for these coronographic data. This procedure relies on the subtraction of the residual light of the occulted star by comparison with a reference star. This subtraction involves a proper centering of both objects and a proper brightness scaling. These parameters are determined so as to minimize the residual signal after subtraction on an assumed
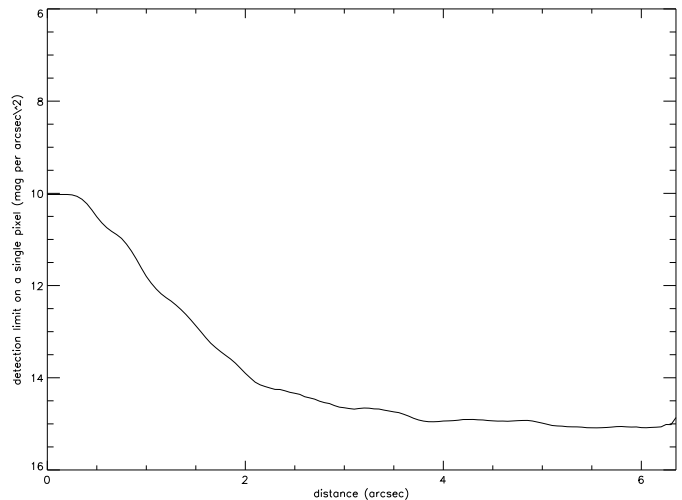

Fig. 4. Detection limit as a function of the star distance, in the case of β Pictoris observations in December 1994, for a total integration time of 6 minutes. Similarly to Fig. 2, it estimates the flux limit detection on a single pixel, expressed in mag arcsec^{-2}.

dust free region, perpendicular to the direction of the disk. This procedure is limited by the S/N ratio of the data and the variability of the PSF. The stability of the PSF provided by the AO system allows a precision of 1/4 pixel (0.012″) for the centering of the reference star, and of 4% for the scaling factor over the 1.5″–6″ range. The corresponding residual signal on a dust free region gives the uncertainty associated to the observations (Fig. 4 and 5). Noticeably, this uncertainty estimation does not only take into account the photon noise and the readout noise (RON), but also, and contrary to previous observations, the uncertainty from the whole reduction procedure. Further than 2″, the dominant errors come from the low flux errors (RON, sky determination and subtraction): a longer total integration time would be necessary to improve this part of the image. Closer than 2″ from the star, errors are mainly due to the subtraction of the comparison star: the uncertainty profile here is a consequence of the photon noise and the intrinsic PSF variability during the on-object integration and during the observation of the reference star.

2.3. Results

2.3.1. Disk detection and orientation

With the present instrumental configuration and exposure times, we detect the disk down to 1.5″ from the star (24 AU) and up to 6″ (100 AU) (Fig. 5).

The disk is detected significantly closer to the star than in previous ground-based observations: Golimowski et al. (1993) and Lecavelier et al. (1993) detected the disk down to 2.4″ (40 AU). Noticeably, our total field of view is enclosed in the numerical mask of the first image of Smith and Terrile (1984). Thus, our data provide complementary informations on the β Pictoris disk.
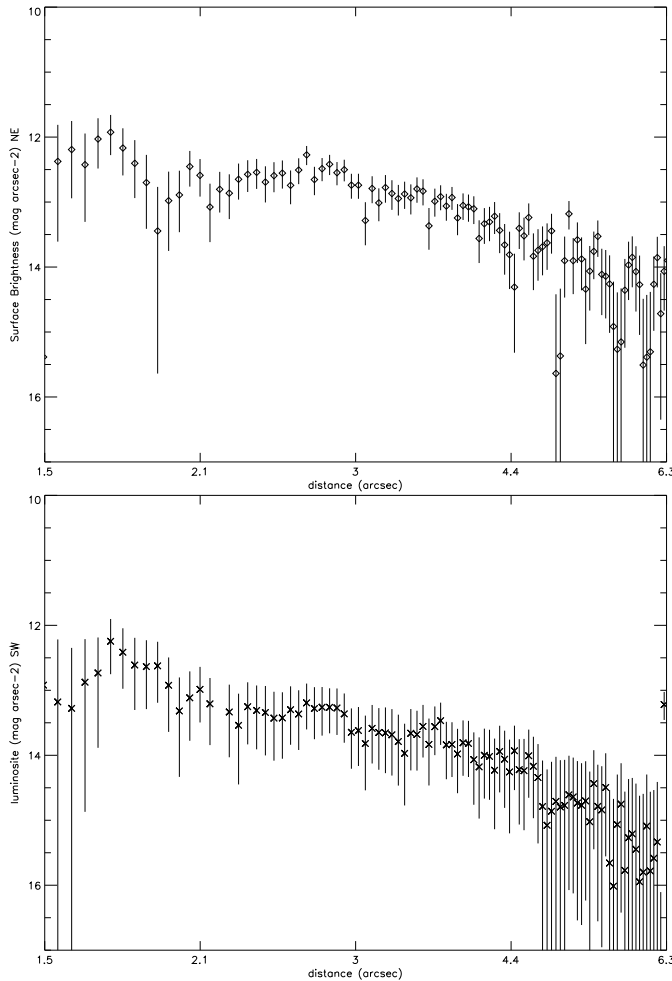
Fig. 6. Radial profiles of the mid-plane SBD obtained on convolved images by a $1''$ seeing profile. This operation strongly increases the S/N but it degrades the angular resolution. The asymmetry between both extensions is constant here over the whole field.

due to an incorrect centering of the reference star: such an error would indeed produce an apparent excess of light on one side of the star, but not so regularly over the $1.5''$–$6''$ range. This asymmetry has already been pointed out by Kalas and Jewitt (1995).

These authors also mentioned a so-called "butterfly asymmetry": the angle formed between the mid-plane line and isophotes is different below and above the disk, and the situation is opposite in both extensions. This effect is also slightly seen here, but a better S/N would be necessary to confirm and quantify this effect.

2.3.3. Vertical distribution

Fig. 7 presents the measured full widths at half maximum (FWHM) of the vertical (perpendicular to the disk orientation) structure of the disk, in both extensions. The FWHM is found to be constant ($1.2'' \pm 0.2''$) over the $2''$–$5''$ range. No asymmetry between the two extensions of the disk is detected.

The constancy of the FWHM along the disk enables us to average the light distribution along the disk axis, so as to derive a mean vertical profile with a good S/N. This averaged vertical profile is found to be better fitted by an exponential law than by a Gaussian one (Fig. 8).

2.4. Comparison with other results

Table 2 summarizes the available results from all the observations performed so far in scattered light imaging. Our observations are confined to the inner part of the disk, from 24 to 100 AU. The overlapping region with previous observations is between 40 and 100 AU. We now compare the different results for the SBD and for the FWHM of the disk.

Fig. 5. Radial profile of the mid-plane SBD of the β Pictoris disk in NE (top) and SW (bottom) extensions. Photometric calibration is performed by comparison with observations of β Pictoris out of the occulted mask. The uncertainties are deduced from rms residual deviation from zero in an emission free region, perpendicular to the disk (Fig. 4). They do not only account for photon noise but also for any variation between the observation of the comparison star and β Pictoris that might affect the result. They apply to each indicated point ; averaging would reduce them.

The NE-SW orientation, $30°$ apart from the North, is in agreement with all observations since 1984.

2.3.2. Surface brightness distribution

Fig. 6 presents the radial dependence of the surface brightness distribution (hereafter SBD). SBD measurements are possible between $1.5''$ and $6''$ from the star.

A single power law poorly fits the SBD over this whole range. Close to the star, the SBD gets flatter, while further out it is steeper. Yet, over the $2''$–$5''$ range, averaged power law index is measured to be -1.3 in both extensions.

A faint asymmetry (0.5 mag), between the NE and SW extensions, is observed in the SBD (Fig. 6). This effect cannot be
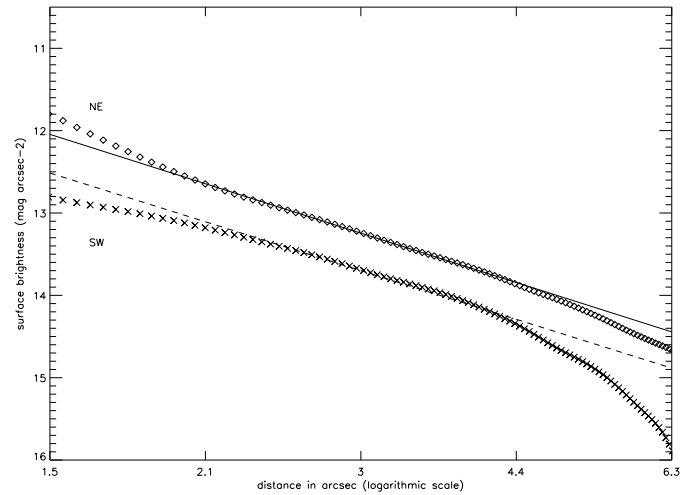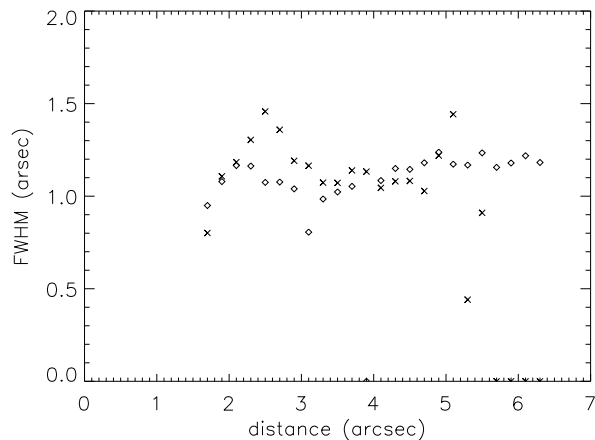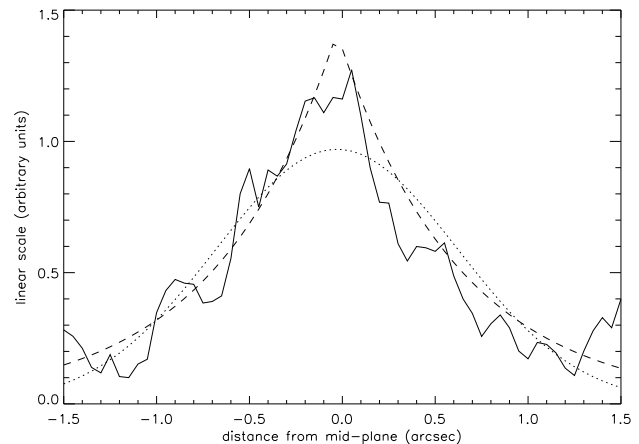
Table 2. Summary of observational results in scattered light imaging

Authors	Correction	Mask	Range	Filter	NE slope	SW slope	FWHM
Smith & Terrile (84)	-	7"	100–400 AU	R	-4.3	-4.3	
Paresce & Burrows (87)	-	4"	100–800 AU	BVRI			
Artymowicz et al. (89)	same data				-3.6	-3.6	increasing with r
Lecavelier et al. (93)	-	–	40–300 AU	BVR	-3.6	-3.6	
Golimowski et al. (93)	tip-tilt	2"	40–100 AU	R	-2.38 ± 0.72	-1.91 ±0.89	32 AU
			100–300 AU		-3.5 ± 0.003	-4.18 ±0.004	increasing with r
Kalas & Jewitt (95)	-	4"	50–100 AU	R	-2.4 ± 0.24	2.47 ± 0.36	36 AU
			100–800 AU		-3.7 ± 0.1	-4.0 ± 0.2	increasing with r
Present data	AO	0.8"	25–40 AU	K'	-1.0 ± 0.8	-1.0 ± 0.8	20 AU
			40- 64 AU		-1.3 ± 0.2	-1.2 ± 0.2	20 AU
			64- 100 AU		-2.5 ± 0.4	-2.9 ± 0.5	20 AU

Fig. 7. Radial dependence on the distance to the star of the disk FWHM. The averaging is here performed along the disk direction to increase the S/N but the vertical sampling is still 0.05″.

Fig. 8. Averaged vertical profile of the disk, perpendicularly to the mid-plane. The exponential fit (dashed line) is better than the gaussian one (dotted line).

2.4.1. Surface brightness distribution

Most of the previous observations are accurate for the outer part of the disk, further than 100 AU. In this area, they consistently show evidence that the mid-plane SBD is very precisely fitted by a steep-power law up to 800 AU, respectively $r^{-3.5}$ and r^{-4} for the NE and SW extensions. Some discrepancies appear among these values but they are not surprising since the given error bars do not take into account all possible reduction biases. The SW extension is slightly steeper and fainter than the NE one.

Closer to the star, between 50 and 100 AU, some data (Golimowski et al. 1993; Kalas & Jewitt 1995) detect a change in the steepness of the disk profile, with flatter indexes of about -2.4. The present data support the previous observation of a flatter disk. But, thanks to the high angular resolution, we can see that the change of slope does not appear abrupt at 100 AU but rather continuous from 100 to 60 AU. The resulting average steepness index is then -2.5 over the 65–100 AU range, and -1.3 over the 40–65 AU range. No slope asymmetry is detected anymore in this area, whereas the SW extension is still slightly fainter.

Actually, the disk seems to continuously become even flatter closer to the star: the measured index over the 25–40 AU range is -0.5. However, this indication should be considered rather qualitatively: this is the place where the stellar light subtraction is delicate and so it might be misleading, similarly to the 40–80 AU range for the non-corrected images.

2.4.2. FWHM

Kalas & Jewitt report that the width of the disk increases with the distance to the star, in the outer region (further than 100 AU), but is constant between 64 and 100 AU from the star. We extend this result down to 32 AU. The thickness they measure is larger than 2″, between 4″ and 6″ from the star. Our present higher angular resolution observations do not confirm this result. We measure a FWHM of 1.2″± 0.2″. This discrepancy is probably due to angular resolution effects, since the convolution by the PSF obviously enlarges the apparent vertical profile of the disk (Fig. 9). The AO PSF is much thinner than the disk FWHM so that the observed vertical profile is not very different from the unconvolved one.
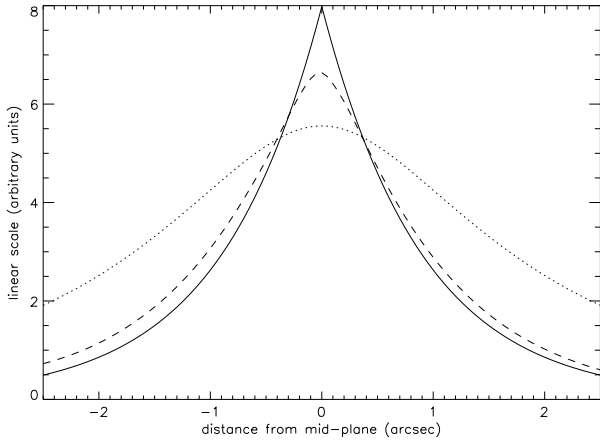
Fig. 9. Effect of the convolution on the vertical profile of a 0.75″ FWHM synthetic disk with different PSF patterns: no convolution (full line), convolution by our instrumental PSF (dashed line), and by a seeing (1″) PSF (dotted line). The FWHM is respectively multiplied by a factor 1.3 and 3.

2.5. Physical parameters

2.5.1. Radial and vertical density distribution

We parameterize the density distribution of particles as done by Artymowicz et al. (1989) and Kalas & Jewitt (1995), assuming an axisymmetric disk described in cylindrical coordinates by:

$$n(r, z) = n(r_0) \left(\frac{r}{r_0} \right)^\alpha exp \left[- \left(\frac{z}{\zeta(r)} \right)^\gamma \right]$$

$$and\ zeta(r) = \zeta_0 \left(\frac{r}{r_0} \right)^\beta.$$

The power-law index α describes the radial decrease of the mid-plane density and γ describes the shape of the vertical decrease. The vertical scale height is driven $\zeta(r)$ and may depend on r through the power-law index β.

Assuming an optically thin disk and an inclination i of the disk, we derive the surface brightness distribution from the density distribution by integration along a line of sight (x, y) of the sky plane, and the convolution by the atmospheric and instrumental PSF:

$$I(x, y) \propto PSF(x, y) * \int_{-\infty}^{\infty} n(r(x, y, l), z(x, y, l)) dl$$

where the proportionality factor involves the total area and the mean scattering efficiency of the grains. To fit our data, we used the PSF measured during the night, closely in time (less than 30 minutes) to the disk observation. As we do not investigate here various possible reasons for brightness asymmetries, we do not take into account anisotropic scattering efficiency.

For the radial density distribution, the free parameters are α, the inner and outer radius. The observed SBD in the 40–65 AU spatial range constrains α between -0. to -0.5. In the inner region, we have to exclude the presence of a sharp inner void

further than 30 AU, as this would induce a sudden change of the SBD slope that is not observed. Thermal IR observations predict the presence of this inner void, within 40 AU, but it still involves some free parameters. This is the first independent, complementary information around the 30 AU range. Between 65 and 100 AU, no single power-law do fit properly the continuous change of SBD index. The density is likely to change rather continuously from the outer steep distribution to the flatter one close to the star. It is then difficult to link these data to previously published ones of the region further out than 100 AU, where a good power-law was observed. Indeed, the SBD is reported to be as steep as -3.5 so that the parameterization has to take into account the precise wings of the seeing PSF. Note that the slope index of typical seeing PSF wings is expected to be about -4.0 or flatter in case of instrumental scattering (Racine 1996), which is unproperly approximated by a Gaussian function as long as the wings are concerned.

For the vertical distribution, β is constrained to be less than 0.5 in order to reproduce the apparent constant FWHM of the SBD. and the scale height is $\zeta(60 AU) = 5$-8 AU, with a small inclination i of the disk between 0 and 5°. The shape of the vertical decrease is poorly constrained: γ between 0.5 and 1.

2.5.2. Mass loss rate

These observations provide important information on the distribution of the material close to the star. Several consequences for the disk can be given. Assuming the given density distribution parameterization, the normal optical thickness is driven by the radial law $\tau(r) \propto r^{\alpha+\beta}$, so that the collision time for these particles is $t_{coll} \propto \frac{P_{orb}}{\tau(r)} \propto r^{3/2-(\alpha+\beta)}$. Finally, the mass loss rate at a given distance to the star is given by

$$\dot{M}(r) \propto \frac{\tau(r)}{t_{coll}} r \propto r^{2(\alpha+\beta)-1/2}$$

so that, after radial integration,

$$\dot{M} \propto \left[r^{2(\alpha+\beta)+1/2} \right]_{r_{min}}^{r_{max}}$$

Then, the density distribution parameters derived here ($\alpha + \beta = 0$) for the inner part of the disk induce a quite different law from the one extrapolated from the outer region ($\alpha + \beta = $ -1.7 to -2). And this induces a mass loss rate 10 time smaller (a few 10^{-14} instead of a few 10^{-13} M$_\odot$yr^{-1}).

2.5.3. Grain size distribution

The multi-wavelength photometry of the disk is related to the scattering efficiency of the grains: according to scattering models (see for instance Chini et al., 1991), this efficiency is constant for wavelengths smaller than the grain size, peaks on a value about 10 times higher at wavelengths comparable to the grain size, and drops to zero for longer wavelengths. Until now, multi-band photometry between B and I (Paresce & Burrows, 1987) has led to the conclusion that the grains in the outer disk are grey scatterers, which means that their size is larger than typically 1

μm (the exact value depending on the precise structure and optical properties of the grains). This lower limit is consistent with the theoretically predicted minimum grain size of 2 μm due to the radiation pressure (Artymowicz, 1988). On the other hand, the mean effective size of the grains is not expected to be much larger either in order to fit with IR data (Backman et al., 1992; Telesco et al., 1988) and polarization measurements (Gledhill, 1991). To directly support all these expectations, colour effects in scattered light should be looked for at slightly longer wavelengths, with a disk brighter by a factor possibly as large as 10, corresponding to the peak scattering efficiency. The present data in K are obtained at wavelengths three times longer than the previous ones in the R band (Kalas and Jewitt, 1995). At 60 AU from the star, where both data have a good S/N ratio, the disk in K appears slightly brighter, by a factor of two. The uncertainties due to the different instrumentations and especially the different angular resolutions (see Sect. 2.4.1.) still keep us from definitely concluding on actual effective grain sizes. Other observations with the same AO system at shorter (down to J band) and longer (L and M bands) wavelengths will greatly improve this constraint, on the close environment of the star.

3. Summary and conclusion

The origin of the strong IRAS excess of the A component of the binary system HR 4796 is still not directly detected in our data; this provides new constraints on the apparent dust luminosity in scattered light down to $2''$ to a 20 mag arcsec^{-2} limit. If the dust shaped a similar disk to that of β Pictoris, it would have been detected. Our constraints, together with the deductions of Jura et al. (1995), suggest a different environment with a confined distribution of dust at a typical distance of 100 AU from the star, and/or a composition of exclusively large grains inefficient at scattering in the near IR. These hypotheses are to be examined in the context of the age of the system and of the vicinity ($7.7''$) of HR 4796B. Thermal IR imaging would bring direct indications to these assumptions.

Meanwhile, IRAS emission excludes the presence of hot dust close to HR 4796A. No companion, which could remove such dust, is either detected down to K = 10 at 40 AU, or K = 14.6 further than 150 AU.

The colour derived spectral type (G0 to G2) indicates that the faint companion HR 4796D at $4.7''$ from HR 4796A, is a background star: this star therefore does not affect the status and evolution of the dust around HR 4796A.

The disk around β Pictoris is detected down to $1.5''$, in high angular resolution ($0.12''$) diffraction-limited K band images. On the $2''$–$6''$ range, we derive a vertical profile of the disk which is well fitted by an exponential law. Its FWHM is shown to be constant and narrow ($1.2''$). The mid-plane surface brightness is much flatter, with a radial index of about -1.3 over the $2''$–$5''$ range, than that observed at larger distances. Previous observations already showed a flattening of the apparent radial brightness distribution closer than 100 AU from the star. The present data show that this flattening carries on even closer to the star, such that the distribution is no longer fitted by a power law.

References

Artymowicz P., 1988, ApJ 335, 79
Artymowicz P., Burrows C., Paresce F., 1989, ApJ 337, 494
Artymowicz P., Clarke C.J., Lubow S.H., Pringle J.E., 1991, ApJ 370, L35
Artymowicz P. & Lubow S.H., 1994, ApJ 421, 651
Backman D.E., Gillet F.C., Witteborn F.C., 1992, ApJ 395, 680
Beuzit J.-L., Mouillet D., Lagrange A.-M., Paufique J., 1997, A&ASS accepted
Burrows, A., Hubbard W.B., Saumon D., Lunine J.I., 1993, ApJ 406, 158
Chini R., Kruegel E., Kreysa E., Shustov B., Tutukov A., 1991, A&A 252, 220
Clarke C. & Pringle J.E., 1991, MNRAS 249, 588
Gledhill T.M., Scarrott S.M., Wolstencroft R.D, 1991, MNRAS 252, 50
Golimowsky D.A., Durrance S.T., and Clampin M., 1993, ApJ 411, L41
Harper D.A., Lowenstein R.F., Davidson J.A., 1984, ApJ 285, 808
Jura M., 1991, ApJ 383, L79
Jura M., Zuckerman, B., Becklin, E.E., 1993, ApJ 418, L37
Jura M., Ghez A.M., White R.J., McCarthy B.W., Smith R.C. and Martin P.G., 1995, ApJ 445, 451
Kalas P., & Jewitt D., 1993, BAAS 25, 1353
Kalas P., & Jewitt D., 1996, AJ 110, 794
Knacke R.F., Fajardo-Acosta S.B., Telesco C.M., Hackwell J.A., Lynch D.K., Russell R.W., 1993, ApJ 418, 440
Koornneef J., 1983, A&A 128, 84
Lagage P.O., Pantin E., 1994, Nature 369, 628
Lagrange A.-M., Plazy F., Beust H., Mouillet D., Deleuil M., Ferlet R., Spyromilio J., Vidal-Madjar A., Tobin W., Hearnshaw J.B., Clark M., Thomas K.W, 1996, A&A 310, 547
Lecavelier A., Perrin G., Ferlet R. et al., 1993, A&A 274, 877
Paresce F. and Burrows C., 1987, ApJ 319, L23
Racine R., 1996, PASP 108, 699
Smith B.A. & Terrile R., 1984, Science, 226, 1421
Telesco C.M., Decher R., Becklin E.E., Wolstencroft R.D., 1988, Nature 335, 51
Zuckerman B., & Becklin E.E., 1993, ApJ 414, 793